Hydrological and Geochemical Monitoring for a CO_2 Sequestration Pilot in a Brine Formation

Christine Doughty, Karsten Pruess, Sally M. Benson, and Barry M. Freifeld
Earth Sciences Division
E.O. Lawrence Berkeley National Laboratory
Berkeley, California, USA

William D. Gunter
Carbon and Energy Management
Alberta Research Council
Edmonton, Alberta, Canada

Abstract

Hydrological and geochemical monitoring are key components of site characterization and CO_2 plume monitoring for a pilot test to inject CO_2 into a brine-bearing sand of the fluvial-deltaic Frio formation in the upper Texas Gulf Coast. In situ, injected CO_2 forms a supercritical phase that has gas-like properties (low density and viscosity) compared to the surrounding brine, while some CO_2 dissolves in the brine. The pilot test employs one injection well and one monitor well, with continuous pressure and flow-rate monitoring in both wells, and continuous surface fluid sampling and periodic down-hole fluid sampling from the monitor well. Pre-injection site-characterization includes pump tests with pressure-transient analysis to estimate single-phase flow properties, establish hydraulic connectivity between the wells, determine appropriate boundary conditions, and analyze ambient phase conditions within the formation. Additionally, a pre-injection tracer test furnishes estimates of kinematic porosity and the geometry of flow paths between injection and monitor wells under single-phase conditions. Pre-injection geochemical sampling provides a baseline for subsequent geochemical monitoring and helps determine the optimal tracers to accompany CO_2 injection. During CO_2 injection, hydrological monitoring enables estimation of two-phase flow properties and helps track the movement of the injected CO_2 plume, while geochemical sampling provides direct evidence of the arrival of CO_2 and tracers at the monitor well. Furthermore, CO_2-charged water acts as a weak acid, and reacts to some extent with the minerals in the aquifer, producing a distinct chemical signature in the water collected at the monitor well. Comparison of breakthrough curves for the single-phase tracer test and the CO_2 (and its accompanying tracers) illuminates two-phase flow processes between the supercritical CO_2 and native brine, an area of current uncertainty that must be better understood to effectively sequester CO_2 in saline aquifers.

Introduction

Geologic sequestration of CO_2 in brine-bearing formations has been proposed as a means of reducing the atmospheric load of greenhouse gases. For this procedure to have any meaningful impact on the global carbon cycle, vast quantities of CO_2 must be injected into the subsurface and isolated from the biosphere for hundreds or thousands of years. To determine whether such an enterprise is feasible and practical requires field-scale testing of CO_2 injection and storage, accompanied by monitoring to verify that the subsurface processes impacting the CO_2 are well understood. Although CO_2 injection has occurred routinely for the past several decades in conjunction with enhanced oil recovery operations, detailed monitoring has been lacking. The upcoming Frio brine pilot (Hovorka et al., 2004) incorporates a variety of monitoring techniques, including hydrological, geochemical, geophysical, and surface methods. The present paper describes hydrological and geochemical monitoring.

Geologic Sequestration in Upper Texas Gulf Coast Saline Aquifers

Brine-bearing formations have been identified as having significant potential nationwide for geologic sequestration of CO_2 (Hovorka et al., 2000). The Frio formation of the upper Texas Gulf Coast is a particularly attractive target, with multiple extensive, thick brine-bearing sand layers containing

significant permeability and porosity at depths suitable for sequestration (>800 m), and an extensive overlying shale layer to serve as a top seal. Additional key features that make the Frio formation well-suited for geologic sequestration include the existence of many localized CO_2 point sources (power plants, refineries, chemical plants), formations that are well characterized due to stratigraphically and structurally analogous petroleum reservoirs, extensive use of the Frio for deep well injection of hazardous waste, and CO_2 injection technology developed for improved oil recovery that has been tested in analogous Gulf Coast formations. Figure 1 shows a portion of the Texas Gulf Coast including the Frio pilot site at the South Liberty oil field.

Frio Pilot Geologic Setting

At the South Liberty field (Figures 2 and 3), the upper part of the Frio formation consists of interleaved sands and shales typical of a fluvial-deltaic environment. Many of the shales are discontinuous lenses, but a thick, regionally extensive shale known as the Anahuac Shale provides a continuous top seal for the Frio sands. Near the top of the Frio at about 1500 m depth is a 25-m-thick sand layer known as the C sand, which is divided by a 0.3-m-thick shale layer into upper and lower zones. Our injection target is the 10-m-thick upper zone of the C Sand, above the thin shale. Sand permeability in this zone ranges from 10 to 150 md, with an average value of 50 md; sand porosity ranges from 20% to 30%, with an average value of 25%. A typical porosity profile inferred from wire-line logs is shown in Figure 4.

The South Liberty field is located on the flank of a salt dome, where the Frio has an average dip of about 15^o. The formation is partially compartmentalized into fault blocks by large sub-vertical faults (Figure 3), with some small faults within the blocks.

The C sand is presumed to be brine-saturated, with total dissolved solids (TDS) estimated to be 100,000, based on regional information. Although the South Liberty field is inactive now, historically hydrocarbons were produced at about 2400 m depth.

Frio Pilot Wells

The Frio Pilot employs two wells, a newly-drilled well to serve as the injection well and an existing well to be recompleted as a monitor well. Both wells will have 5½-inch casings, and be perforated over the C sand interval. Packers will isolate the C sand from overlying and underlying layers. The injection well will use 2 7/8-inch injection tubing. The target separation for the two wells is 30 m, with the injection well sited directly down-dip (south) of the monitor well.

Flow and Transport Processes

We plan to inject 3,750 tonnes of CO_2 over a two-week period. The nominal injection rate will be 250 tonnes/day, which is roughly equivalent to 50 gpm. Ambient reservoir conditions are expected to be about $T = 64^oC$ and P = 150 bars. The critical point of CO_2 is $T = 31^oC$ and P = 73.8 bars, implying that in situ CO_2 will form a supercritical phase and partially dissolve in the aqueous phase (brine). The supercritical phase is gas-like in that it is less dense and less viscous than the surrounding brine. Here, we refer to the supercritical phase simply as gas. Dissolved CO_2 slightly increases the density of the brine, resulting in the interesting dynamic that gas-phase and dissolved-phase CO_2 experience opposite buoyancy forces.

We use the numerical simulator TOUGH2 (Pruess et al., 1999) with a special fluid property module for CO_2-brine mixtures (Pruess and Garcia, 2002) to model the multi-phase, multi-component flow and transport processes arising from injection of CO_2. The porosity profile shown in Figure 4 provides the fundamental information for deriving other flow properties such as permeability and characteristic curve parameters. Figure 4 also shows the discretized representation of the porosity profile used for the three-

dimensional numerical model of the C sand. The model extends laterally over the fault block shown in Figure 3.

In the subsurface, CO_2 moves under the combined effects of pressure gradients and gravity away from the injection well. Based on numerical simulations, it is expected to reach the monitor well in 3-6 days. Figure 5 shows the modeled initial pressure distribution and Figure 6 shows a series of snapshots of the gas-phase CO_2 plume during the 15-day injection period.

Overview of Frio Pilot Monitoring

The monitoring for the Frio pilot can be divided into four categories: hydrological, geochemical, geophysical, and surface. Hydrological monitoring encompasses pressure and flow-rate measurements. Geochemical monitoring includes collection of both down-hole and surface samples from the wells. An on-site portable quadrupole mass spectrometer will be used for real-time analysis of collected samples, to provide preliminary results and temporal guidance on sampling for off-site laboratory analyses. Further details of hydrological and geochemical monitoring programs are given in the following two sections.

Geophysical monitoring includes the following three components: a neutron probe placed in the monitor well to identify the arrival of the gas-phase CO_2 plume; cross-well seismic surveys using the injection and monitor wells, conducted before and after CO_2 injection, to study the distribution of CO_2 in the plane of the two wells; and vertical seismic profiling (VSP), conducted after CO_2 injection to investigate the spatial distribution of the CO_2 plume.

Surface monitoring searches for evidence of leakage (to the shallow subsurface and seepage out of the ground (Oldenburg and Lewicki, 2003). The surface monitoring program for the Frio pilot will collect soil-gas samples, measure CO_2 soil flux, and CO_2 soil-gas concentration profiles with depth. Sample collection locations will focus on two types of potential leakage pathways: man-made structures such as damaged or abandoned wells, and natural geological features such as faults and outcrops. Because CO_2 from the Frio pilot is not expected to reach the surface, it is critical to do pre-CO_2 baseline monitoring to identify the CO_2 signature of naturally-occurring processes.

Monitoring Prior to CO_2 Injection - Site Characterization Activities

The site-characterization goals of pressure-transient testing are to estimate single-phase flow properties, test for hydraulic connectivity between wells, characterize boundaries, and analyze the ambient phase conditions within the formation. Figure 7 shows the pressure-transient response at both wells when fluid is produced from the injection well at a rate of 45 gpm. To analyze the effect of different assumptions about flow across faults, three different cases are considered for the small fault to the north of the wells (other faults bounding the compartment (Figure 3) are far enough away so that their flow properties do not significantly affect a few-day-long well test):

- Fault is closed (a no-flow boundary)
- Fault is absent
- Fault is open (a constant-pressure boundary)

The different fault assumptions have a small effect on the late-time portion of the pressure transient, with the closed fault producing the largest pressure response and the open fault producing the smallest. Removing the thin shale layer within the C sand has a bigger effect on the pressure response, decreasing it by about 2-3 bars.

Although the C sand is nominally considered to be brine-saturated, its proximity to petroleum resources makes it possible that dissolved or immobile gas (methane) may be present. The key feature enabling gas to be identified from pressure-transient testing is that it has a much larger compressibility than liquid. If only dissolved gas is present, the initial pressure decrease in response to a pump test will be rapid, reflecting the small compressibility of a pure liquid phase (along with rock compressibility, which is also small). If pressure decreases enough for degassing to occur, the compressibility becomes

much larger, and the pressure response slows correspondingly. If immobile gas is present under ambient conditions, the initial pressure decrease will be slow, and as additional degassing occurs, the response will slow further.

The analysis procedure is as follows. We assume compressibility is additive:

$C = C_r + S_l C_b + S_g C_g$

where C is total compressibility, C_r is rock compressibility, S_l and $S_g = (1 - S_l)$ are liquid- and gas-phase saturations, respectively, and C_b and C_g are brine and gas compressibilities, respectively. For an ideal gas, $C_g = 1/P$. Using standard analysis techniques, the y-intercept of the late-time portion of a log-linear plot of pressure change as a function of time determines C. With C_b and C_g known, we can infer gas saturation under ambient conditions and after degassing has occurred. Figure 8 illustrates the procedure for a hypothetical case with 10% immobile methane ($S_g = 0.10$) originally in place. Early on, before the pressure has decreased enough for much degassing to occur, $C = 1.4 \cdot 10^{-8}$ Pa^{-1}, 3.5 times bigger than the comparable value for a brine-saturated system, and the corresponding gas saturation is $S_g = 0.11$. After about one hour, pressure has decreased enough for substantial degassing to occur around the well, yielding about a factor of two increase in C, and $S_g = 0.25$.

In addition to pressure-transient testing, site-characterization activities will include a tracer test, employing a conservative solute (fluorescein) in a balanced doublet (injection rate at the injection well equals pumping rate at the monitor well) to create a steady flow field between the injection and monitor wells. A tracer-test breakthrough curve has three main attributes of interest: the time of first arrival, the peak concentration, and the overall shape of the curve. The time of first arrival determines the velocity through the fastest flow paths. The average time of arrival, in conjunction with the injection rate, permits an estimation of the volume through which the tracer flowed. For a single-phase tracer test, this volume is simply the connected pore space, as measured by the porosity (sometimes denoted the kinematic porosity to emphasize that it measures the volume through which flow occurs). For a multi-phase tracer test (essentially what we are doing when we inject CO_2), this flow volume is measured by the product of porosity and tracer-phase saturation (the saturation of the phase in which the tracer exists). Thus, in order to infer mean gas saturation from gas-phase CO_2 arrival, we need to have an independent estimate of porosity, hence the motivation for the single-phase tracer test. Additionally, the overall shape of the breakthrough curve provides information on the distribution of flow paths (for example, uniform versus strongly preferential flow). If breakthrough curve shape differs between single-phase and multi-phase tracer tests, this provides us with information on the changes in flow paths arising from multi-phase effects.

Figure 9 shows the modeled response for a tracer test sequence consisting of:

- Days 0-2: pump at monitor well
- Days 2-4 pump and inject as a balanced doublet, establish steady flow field
- Day 4: add tracer slug at injection well
- Day 4 onward: record breakthrough curve (BTC) at monitor well

Results suggest that initial tracer breakthrough will be rapid, occurring within several days. Different assumptions about flow conditions at the small fault north of wells do not affect results strongly.

The final component of site-characterization activities is to collect minimally disturbed down-hole samples, in order to establish baseline geochemistry. An understanding of in situ conditions will help determine the optimal tracers to accompany CO_2 injection.

Monitoring During CO_2 Injection

Continuous hydrologic monitoring (pressure and flow rate) will occur at both the injection and monitor wells to estimate two-phase flow properties and help track the movement of the injected CO_2 plume. Geochemical sampling at the monitor well will provide direct evidence of breakthrough of CO_2 and tracers. Moreover, CO_2-charged water acts as a weak acid, and reacts to some extent with the minerals in the aquifer, producing a distinct chemical signature in the water collected at the monitor well.

We plan to add a unique tracer to all fluids that are introduced into the subsurface as part of the pilot test (CO_2, drilling mud, well-completion cement, etc). Thus, collected samples will contain an easily detectable signature, facilitating a reconstruction of fluid movement and interactions. A novel small-diameter u-tube sampling system with a down-hole check-valve will be deployed to produce samples at the surface. A high-pressure separator and manifold at the surface will allow independent analysis of liquid and gaseous components. This sampling system will be augmented by collecting periodic down-hole samples. The main criterion for sampling methodology is to allow accurate recreation of down-hole conditions. Real-time tracer analysis will be performed at the surface using a portable quadrupole mass spectrometer.

The proposed CO_2 injection schedule consists of several periods of constant-rate injection interspersed with rest periods in which injection and monitor-well pumping are halted. The pressure-transient response to the cessation and resumption of injection will reflect two-phase conditions around the injection well, and by modeling them we hope to learn more about two-phase flow processes. The present plan is to incorporate two distinct rest periods, one early in the injection schedule, when the two-phase CO_2 plume is small, and another late in the injection schedule, when the plume is large, so that the pressure-transients for different two-phase volumes can be compared.

Results of numerical simulations considering a simpler injection schedule with just one rest period (four days injection, two days of rest, eleven days of injection) are shown in Figures 10 and 11. Two cases are considered, assuming different values of residual phase saturations. Residual gas saturation plays a strong role in controlling two-phase flow processes, as discussed further in the next section. The models predict that dissolved CO_2 reaches the monitor well in two to three days for both cases, before the rest period begins. For Case 1, the gas-phase CO_2 lags behind the dissolved phase, and does not reach the monitor well until after injection resumes after the rest period (the net transit time is five to six days). In contrast, for Case 2, the gas-phase CO_2 follows the dissolved phase closely, reaching the monitor well in about three days. Note that after the gas phase arrives at the monitor well, the flowing fraction of gas phase (down hole, at the sand face) does not equal the in situ gas saturation, because flow depends on fluid mobility rather than saturation.

Fundamental Information from Hydrological and Geochemical Monitoring

Two-phase flow processes (i.e., how two phases interact and interfere) for the supercritical CO_2 /native brine system are poorly understood. Mathematical models use relative permeability and capillary pressure functions to account for two-phase flow processes, and the appropriate functional forms and parameters for these functions must be provided. In particular, residual gas saturation (the saturation below which the gas phase is immobile) has a strong impact on CO_2 plume behavior. For example, for the results shown in Figures 10 and 11, Case 1 uses a residual gas saturation of $S_{gr} = 0.24$, whereas Case 2 uses $S_{gr} = 0.05$. Figure 12 shows the relative permeability curves corresponding to these values of S_{gr}. The domain of saturation over which the gas-phase CO_2 plume has significant mobility differs greatly for the two cases: for Case 1 the gas-phase becomes mobile at lower values of liquid saturation S_l than for Case 2, corresponding to higher values of gas saturation S_g. Thus, more gas-phase CO_2 must be added to the system for the Case 1 plume to move as readily as the Case 2 plume. The net result is a more compact CO_2 plume with a higher value of gas saturation S_g for Case 1, which does not move away from the injection well as rapidly as for Case 2, yielding a later arrival time at the monitor well.

Residual phase saturation depends in part on features of pore-scale geometry and on the wettability of the fluids present, and as such is amenable to laboratory-scale studies using core samples. However, core-scale studies cannot predict how the different phases will interact and interfere at the field scale, where larger-scale aspects of geologic heterogeneity come into play. Thus, to obtain reliable values for residual gas saturation, we have to study field-scale behavior. The Frio pilot provides us with three opportunities to do just this:

- Comparison of pressure-transients during single-phase well-tests and during CO_2 injection,
- Comparison of breakthrough curves for single-phase tracer test and CO_2,
- Comparison of breakthrough curves for CO_2 and co-injected tracers.

In addition to enabling us to better understand the two-phase flow processes occurring during the pilot test, developing an improved understanding of how residual phase saturation impacts CO_2 plume evolution has important ramifications for developing successful strategies for sequestration in general. Note from Figures 10 and 11 that the gas saturation within the CO_2 plume is significantly higher for Case 1 than for Case 2. Gas saturation essentially describes how efficiently the CO_2 is stored in the pore spaces (with the remainder of the pore space ($S_l = 1 - S_g$) remaining brine-filled). Thus it impacts directly the capacity of the subsurface to store CO_2. Even more importantly, differences in residual gas saturation control differences in the long-term mobility of the CO_2 plume. Figures 13 and 14 show the results of long-term numerical simulations following the Frio pilot fifteen-day CO_2 injection period, for Cases 1 and 2. The difference in plume mobility is striking. For Case 1, the plume becomes essentially immobile soon after injection ceases, and the plume spreads enough for S_g to drop to S_{gr}. In contrast, for Case 2 the plume remains mobile for long times, moving upward through the formation in response to buoyancy forces. As the plume moves, the gas contacts more brine, enabling more CO_2 to dissolve.

Both Case 1 and Case 2 may represent successful sequestration strategies: in Case 1, we have a "sticky" plume that remains trapped in place, whereas in Case 2, we have a "slippery" plume that gradually dissolves as it moves. However, in order to assess subsurface capacity for storage and risks involved with different kinds of plumes, we must know which scenario is likely to develop for given geological conditions. The hydrological and geochemical monitoring for the Frio pilot will provide the basis for analyses aimed at that very issue.

Acknowledgement

We thank Curt Oldenburg and Kenzi Karasaki for their careful reviews of this paper. This work was supported as part of the GeoSeq project by the Assistant Secretary for Fossil Energy, Office of Coal and Power Systems and the Office of Natural Gas and Petroleum Technology, through the National Energy Technology Laboratory; and the Director, Office of Science, Office of Basic Energy Sciences, of the U.S. Department of Energy under Contract No. DE-AC03-76SF00098.

References

Hovorka, S.D., M.L. Romero, A.G. Warne, W.A. Ambrose, T.A. Trembley, R.H. Treviño, and D. Sasson, Sequestration of greenhouse gases in brine formations, http://www.beg.utexas.edu/CO2/, 2000.

Hovorka, S.D., M.H. Holtz, L.R. Myer, and C. Doughty, Frio brine pilot carbon sequestration project – status report, Third Annual Conference on Carbon Sequestration, National Energy Technology Laboratory, Alexandria, Virginia, May 3-6, 2004.

Oldenburg, C.M. and J.L. Lewicki, Near-surface monitoring strategies for geologic carbon dioxide storage verification, LBNL-54089, Lawrence Berkeley National Laboratory, Berkeley, California, 2003.

Pruess, K., C.M. Oldenburg, and G.J. Moridis, TOUGH2 user's guide, Version 2.0, Rep. LBNL-43134, Lawrence Berkeley National Laboratory, Berkeley, California, 1999.

Pruess, K. and J. García, Multiphase flow dynamics during CO2 injection into saline aquifers, *Environmental Geology*, 42, 282 - 295, 2002.

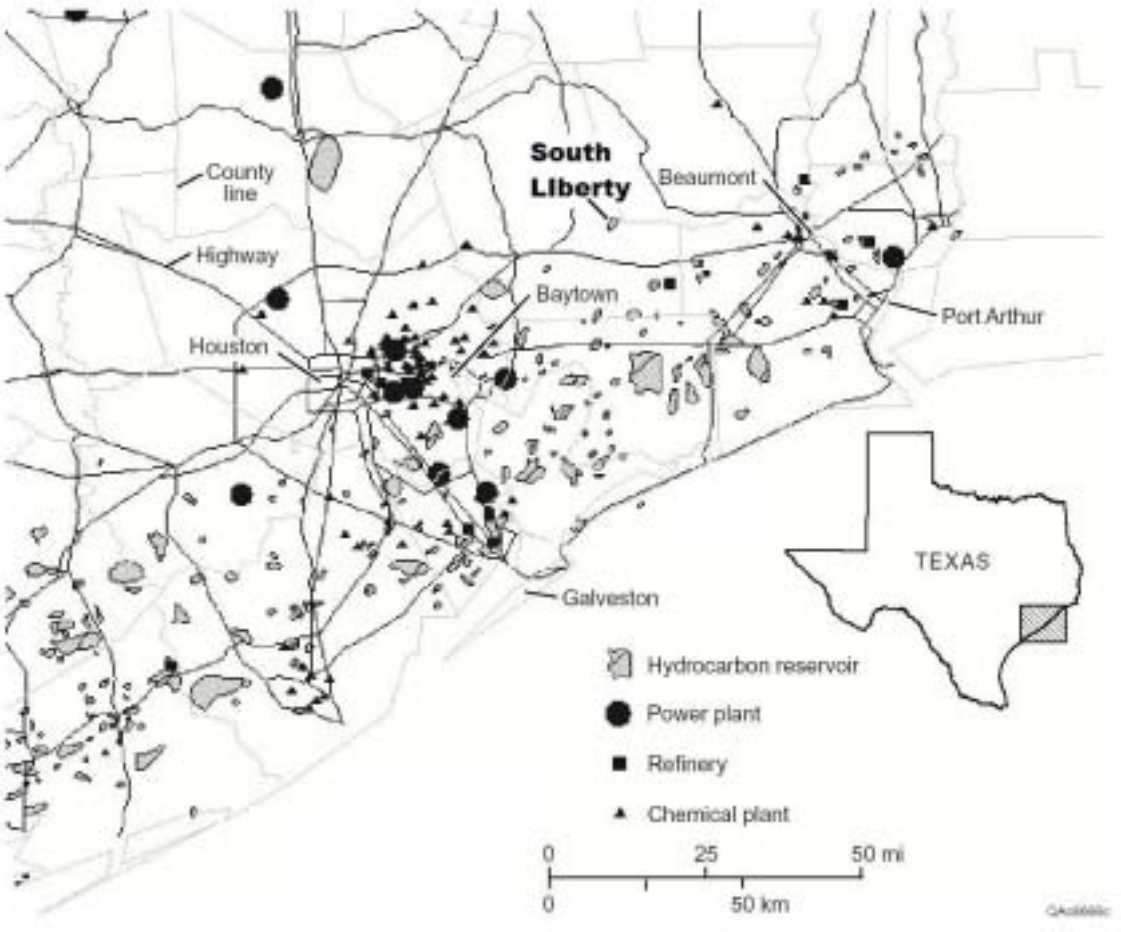

Figure 1. The Texas Gulf Coast including the Frio pilot site at the South Liberty field.

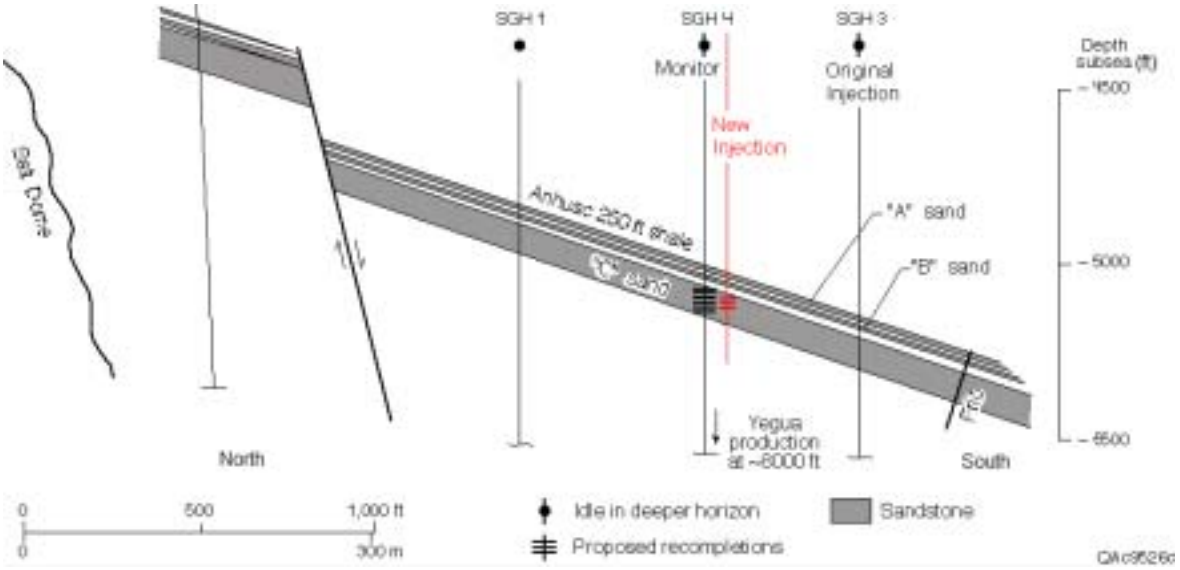

Figure 2. North-South cross-section through the upper part of the Frio formation at the pilot site at the South Liberty field, showing the target C sand, the overlying A and B sands, and the regional seal formed by the Anahuac shale.

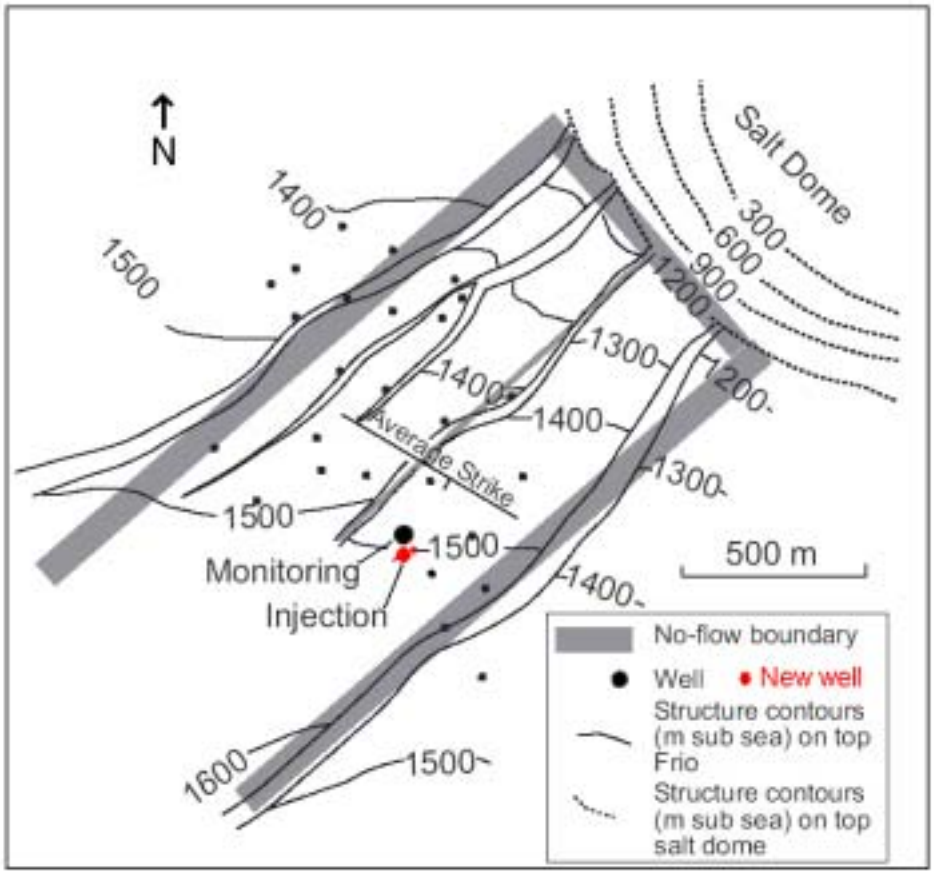

Figure 3. Plan view of the Frio pilot site at the South Liberty field, showing the compartmentalizing faults and their representation as no-flow boundaries in the numerical model.

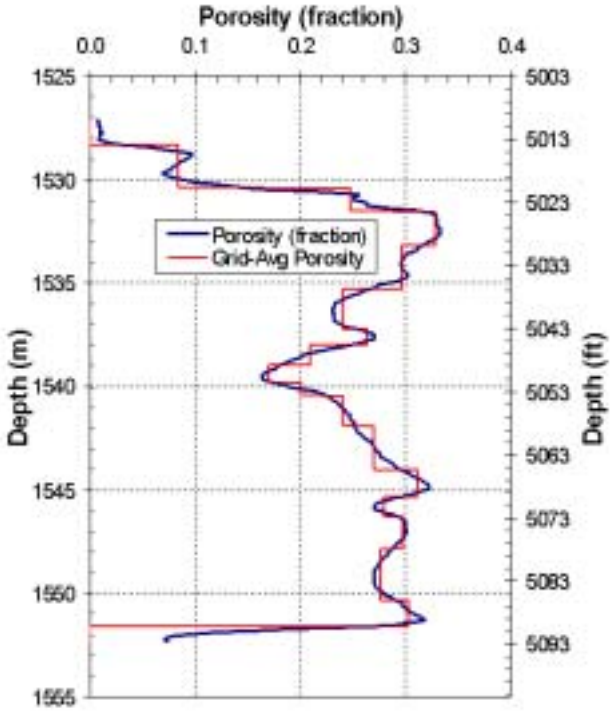

Figure 4. Porosity versus depth profile for the monitor well, and the grid-averaged values used for the numerical model. The CO_2 injection interval is at 1530-1540 m depth.

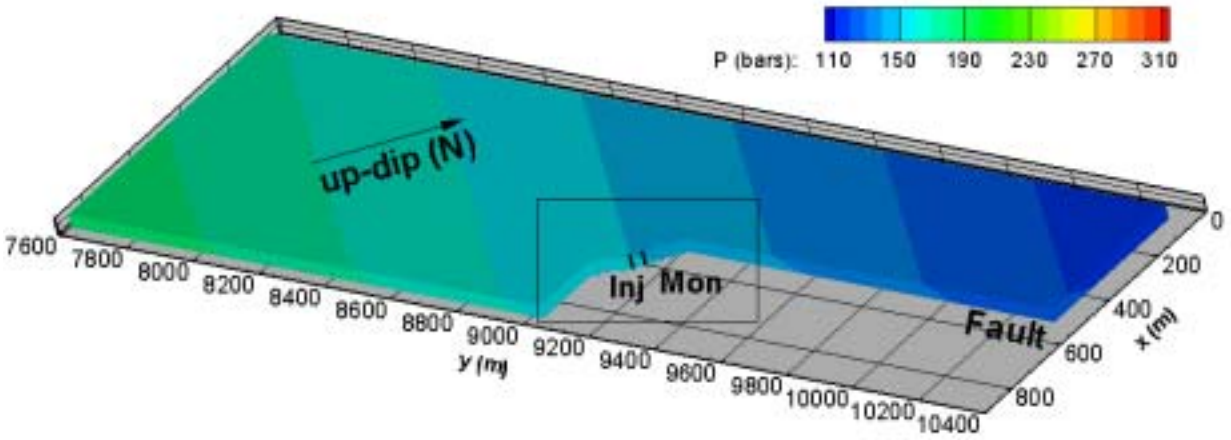

Figure 5. Cut-away view of the initial pressure distribution in the model of the C sand at the Frio pilot site. The cut exposes the line between the injection and monitor wells, and then follows the small fault to the north of the wells.

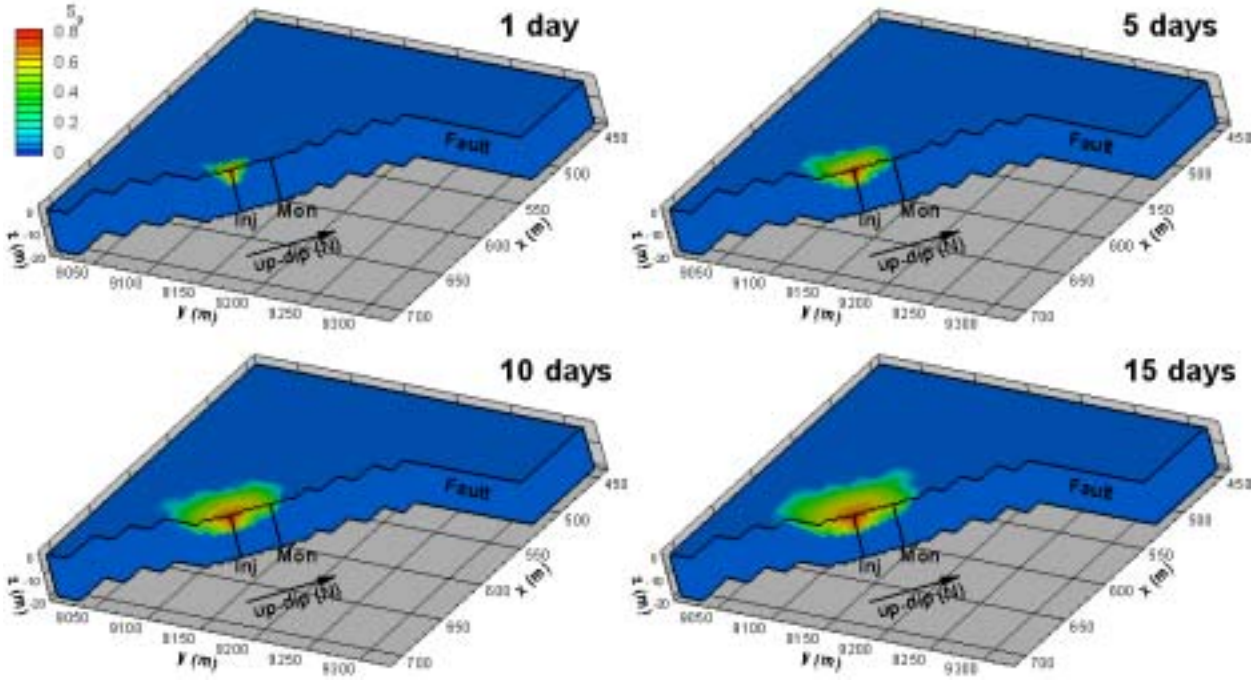

Figure 6. Cut-away view of the modeled gas saturation (S_g) distributions in the C sand at a series of times during the two-week CO_2 injection period. The top three meters of the C sand are removed to enable the maximum extent of the CO_2 plume to be shown.

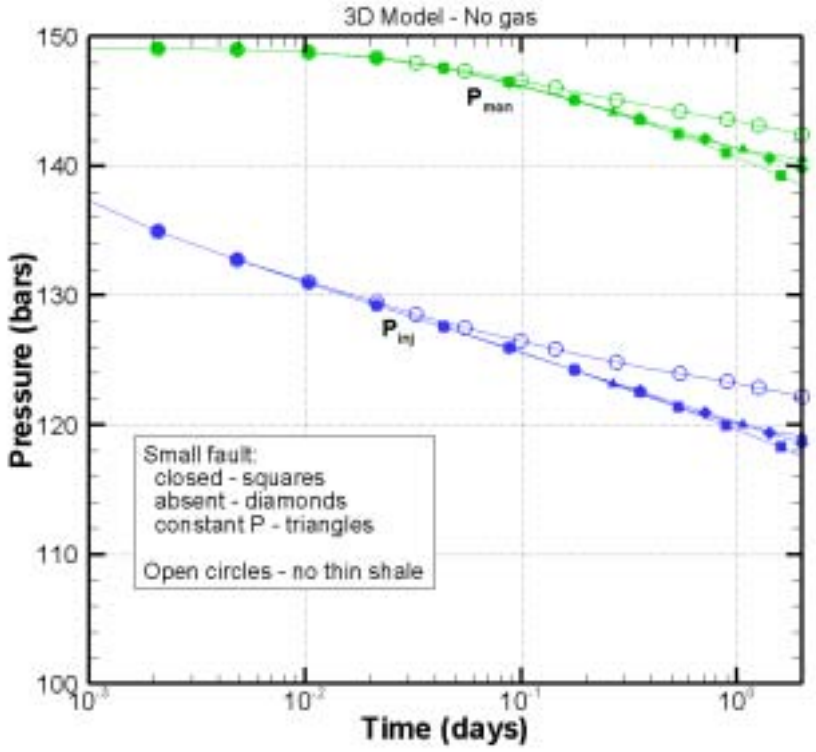

Figure 7. Modeled pressure-transient response during a site-characterization pump test. The pressure response to pumping at the injection well is shown for three different assumptions about the flow properties of the small fault to the north of the wells and assuming there is no thin shale layer within the C sand.

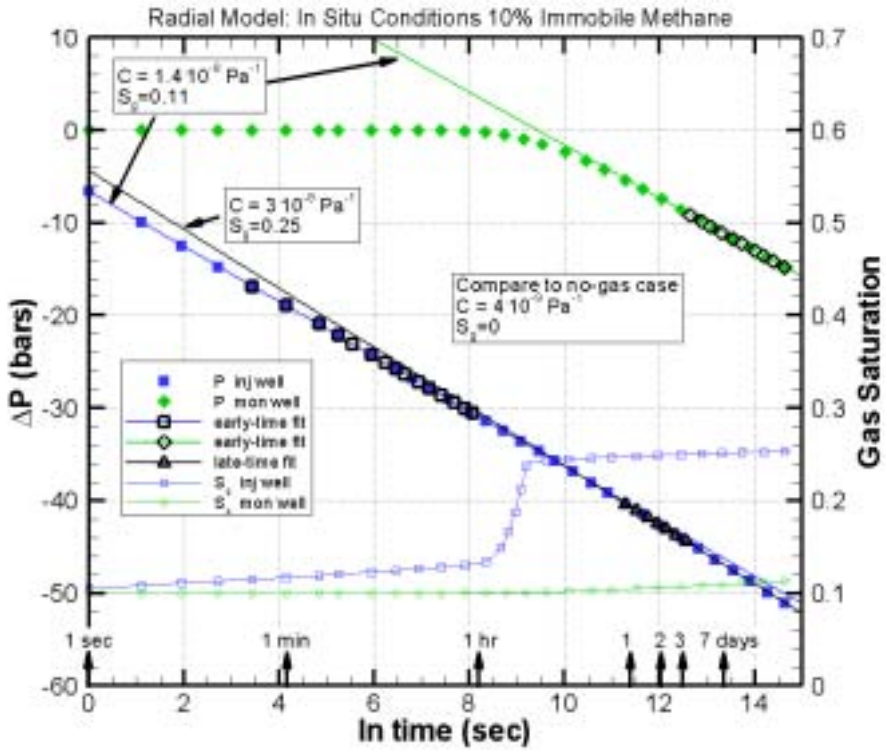

Figure 8. Radial-model pressure-transient response illustrating the curve-fitting technique used to infer the value of effective formation compressibility.

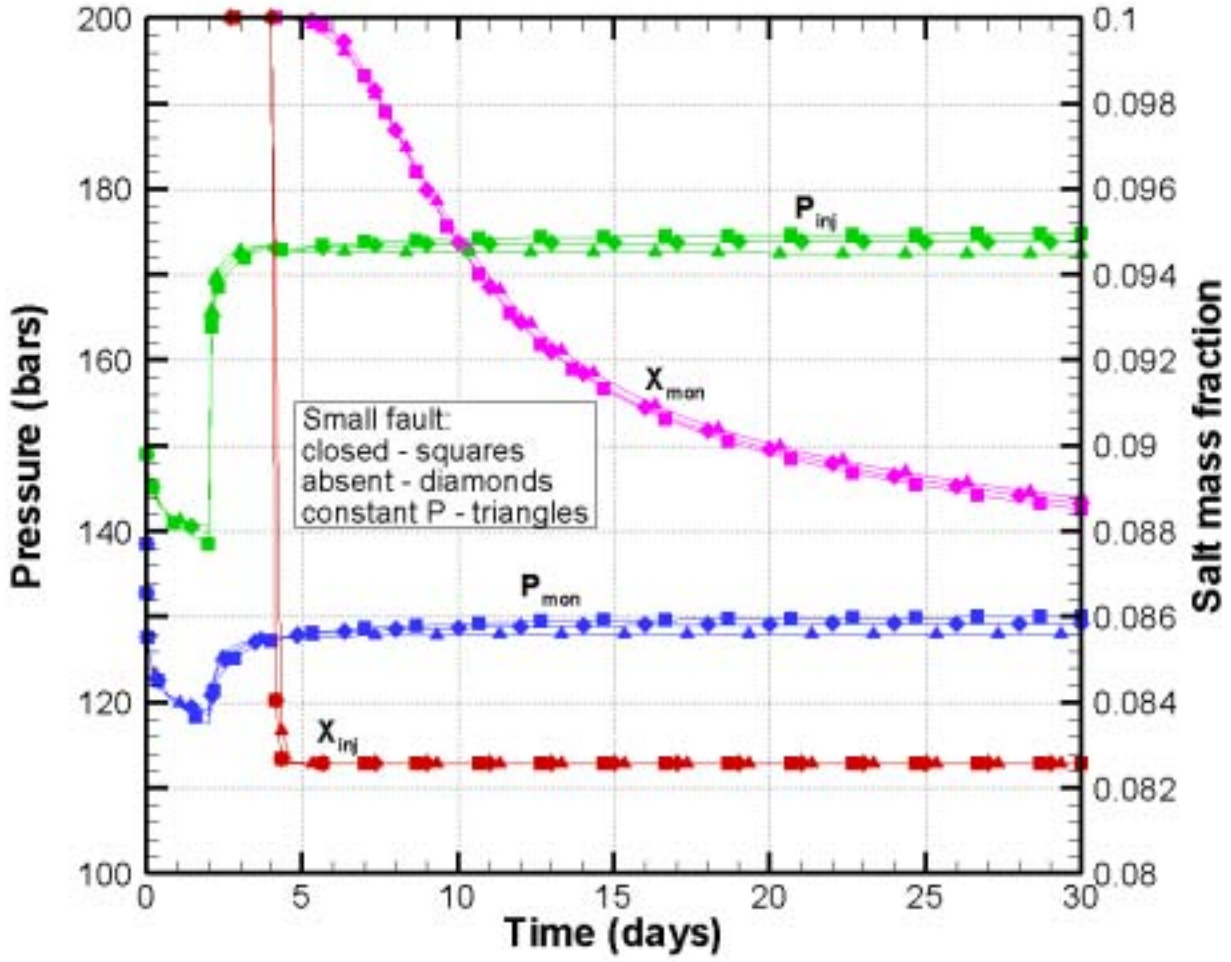

Figure 9. Modeled pressure (P) and concentration (X) response to the site-characterization tracer test.

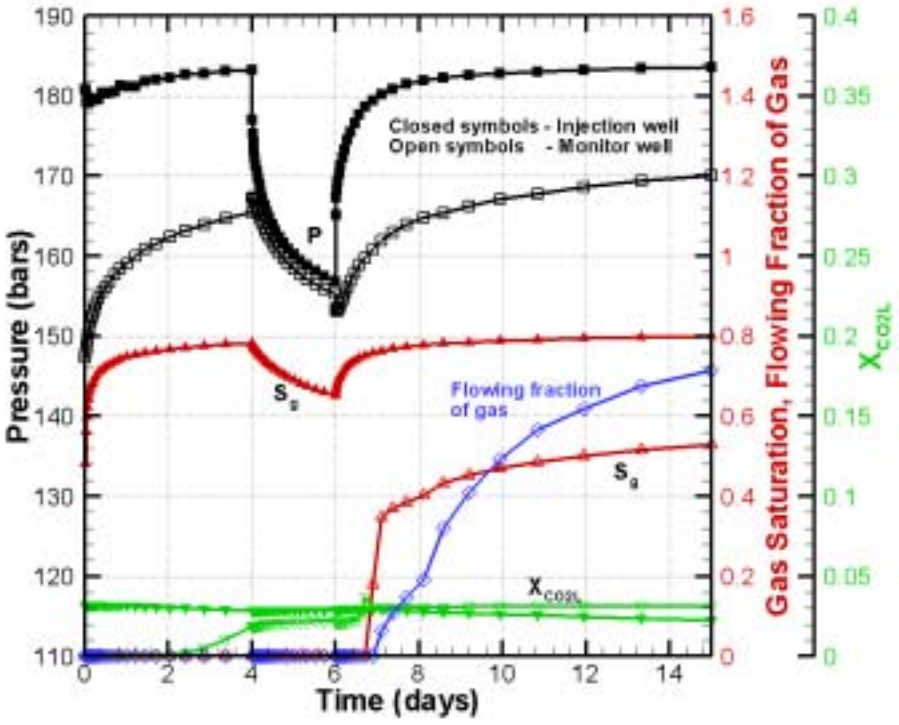

Figure 10. Modeled pressure (P), gas saturation (S_g), and dissolved CO_2 mass fraction (X_{CO2L}) during a 15-day CO_2 injection period containing a two-day rest, for Case 1. The flowing fraction of gas at the monitor well is also shown.

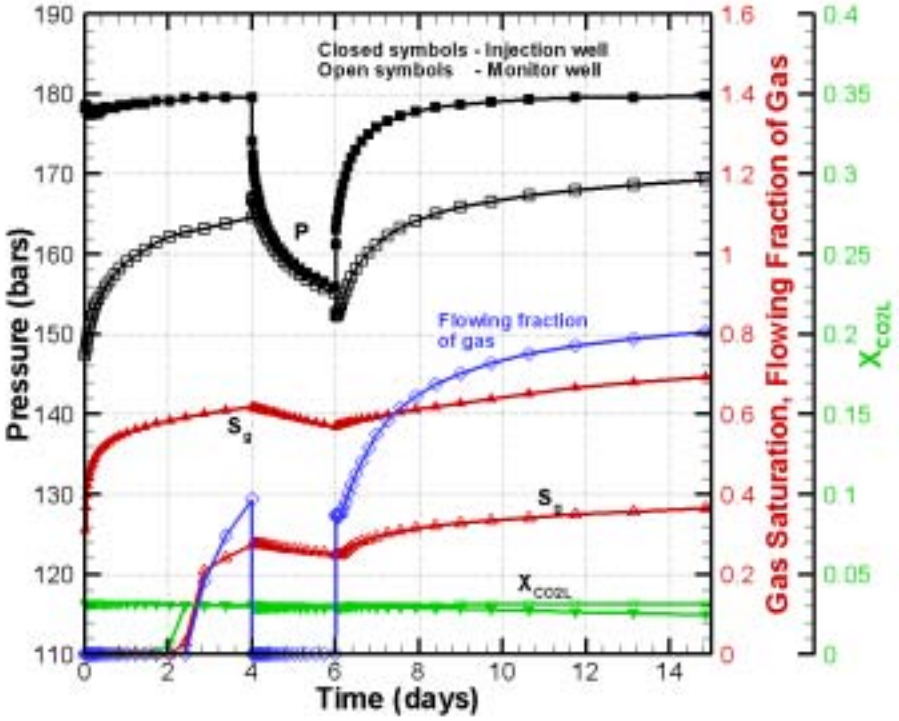

Figure 11. Modeled pressure (P), gas saturation (S_g), and dissolved CO_2 mass fraction (X_{CO2L}) during a 15-day CO_2 injection period containing a two-day rest, for Case 2. The flowing fraction of gas at the monitor well is also shown.

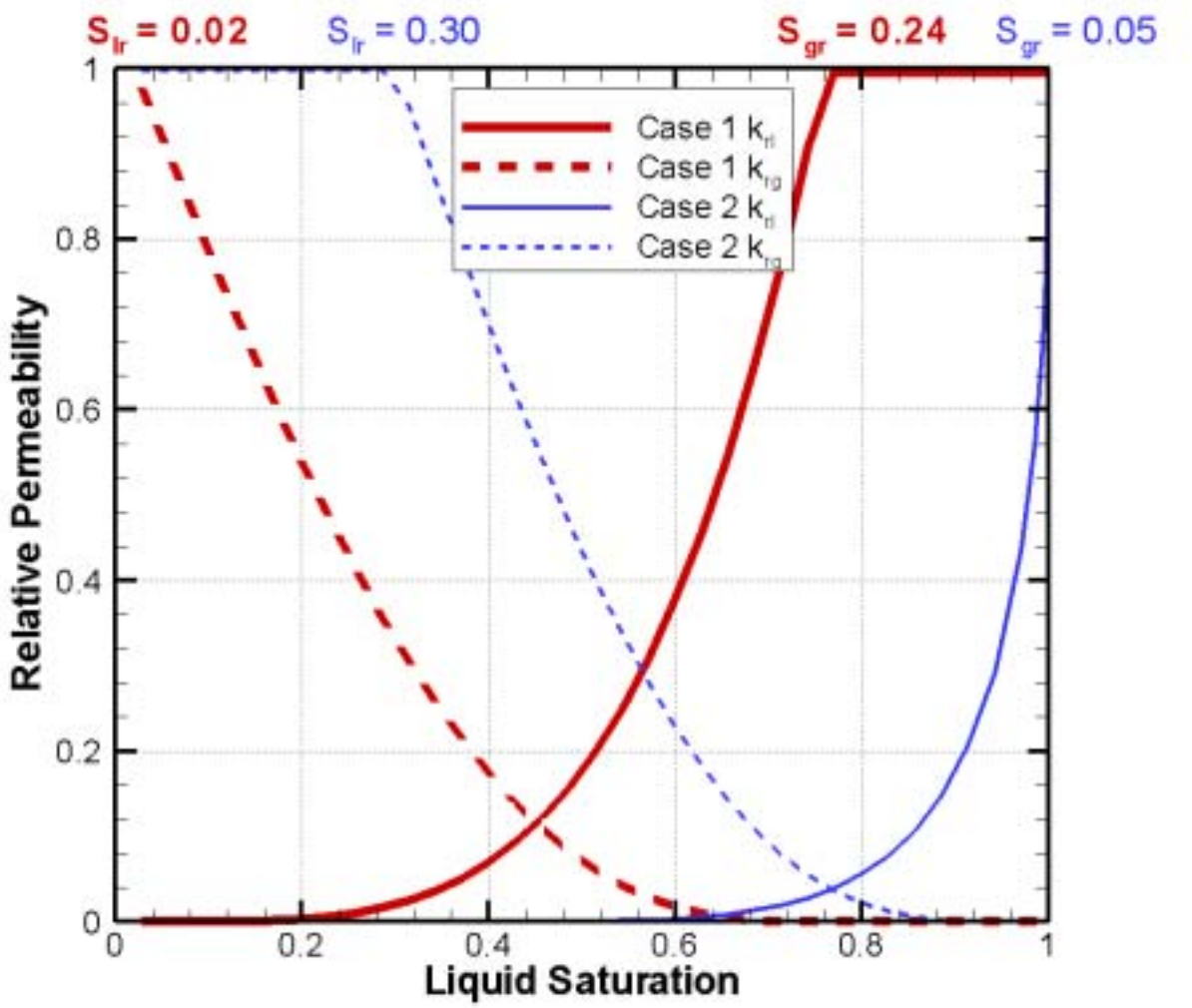

Figure 12. Relative permeability functions with the different values of residual phase saturation used for Case 1 and Case 2 models.

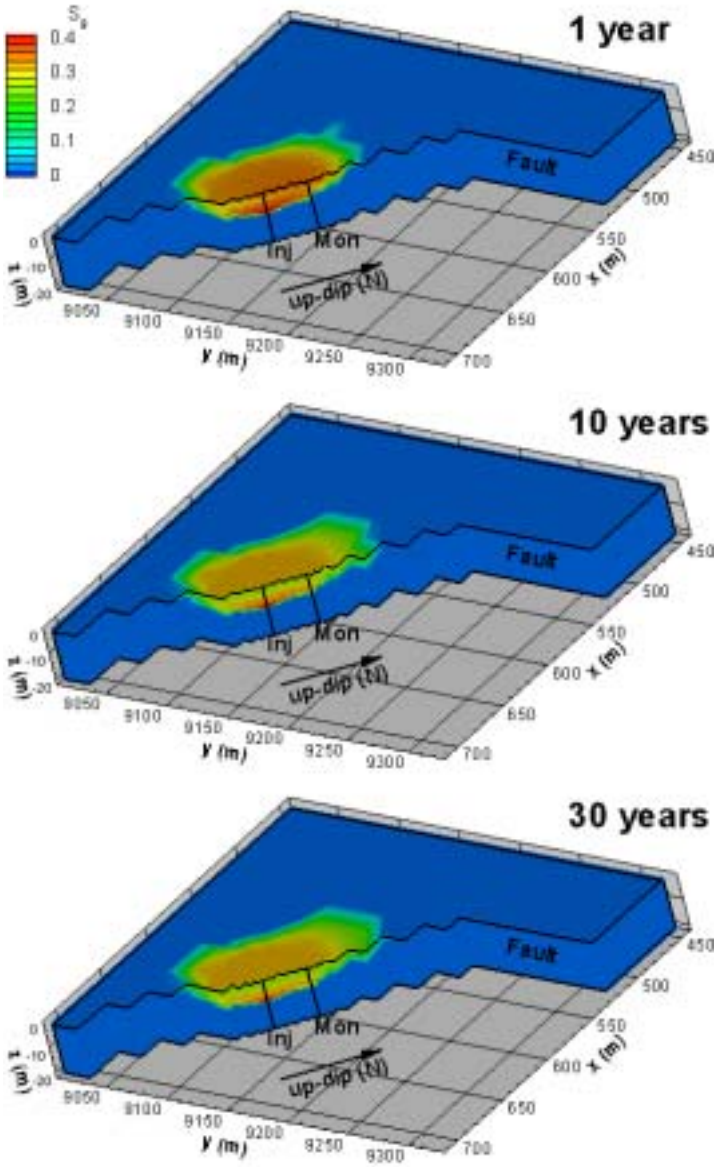

Figure 13. Cut-away view of the modeled gas saturation distributions in the C sand at different times after the 15-day CO_2 injection period has ended, for Case 1. The top two meters of the C sand are removed to enable the maximum extent of the CO_2 plume to be shown.

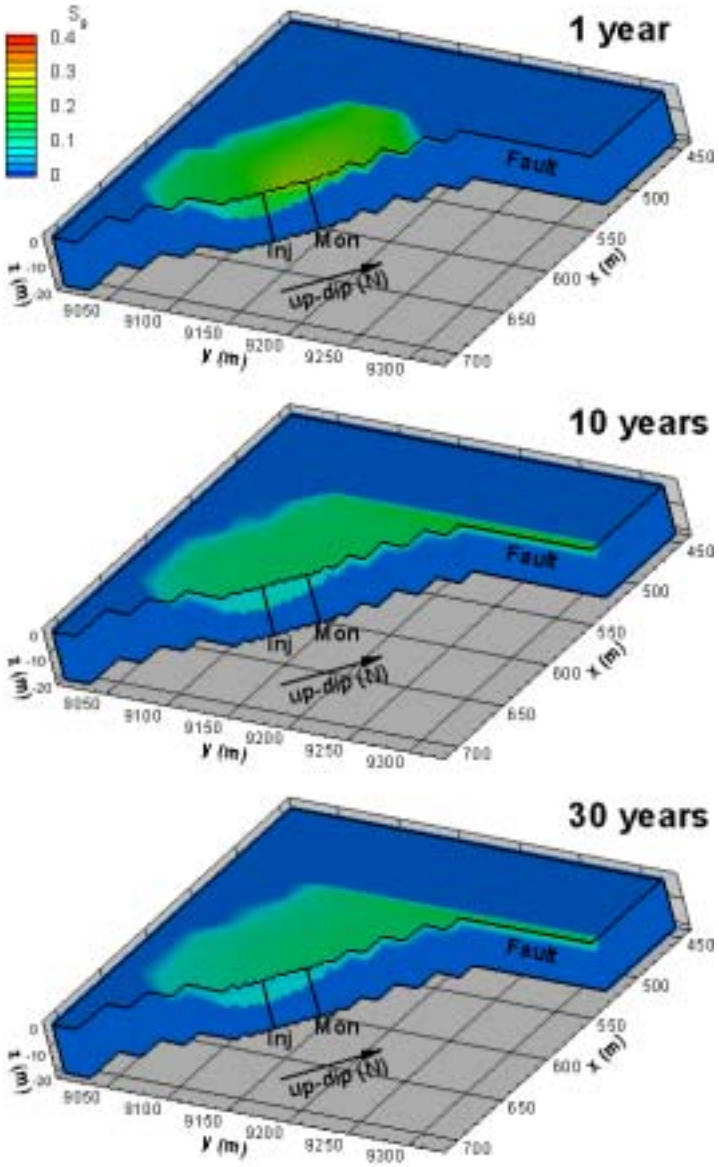

Figure 14. Cut-away view of the modeled gas saturation distributions in the C sand at different times after the 15-day CO_2 injection period has ended, for Case 2. The top two meters of the C sand are removed to enable the maximum extent of the CO_2 plume to be shown.